Science Advances
AAAS

Supplementary Materials for

Astrocyte dysfunction drives abnormal resting-state functional connectivity in depression

Jiaming Liu *et al.*

Corresponding author: Ed X. Wu, ewu@eee.hku.hk; Yanqiu Feng, foree@smu.edu.cn;
Xiong Cao, caoxiong@smu.edu.cn

Sci. Adv. **8**, eabo2098 (2022)
DOI: 10.1126/sciadv.abo2098

The PDF file includes:

Other Supplementary Material for this manuscript includes the following:

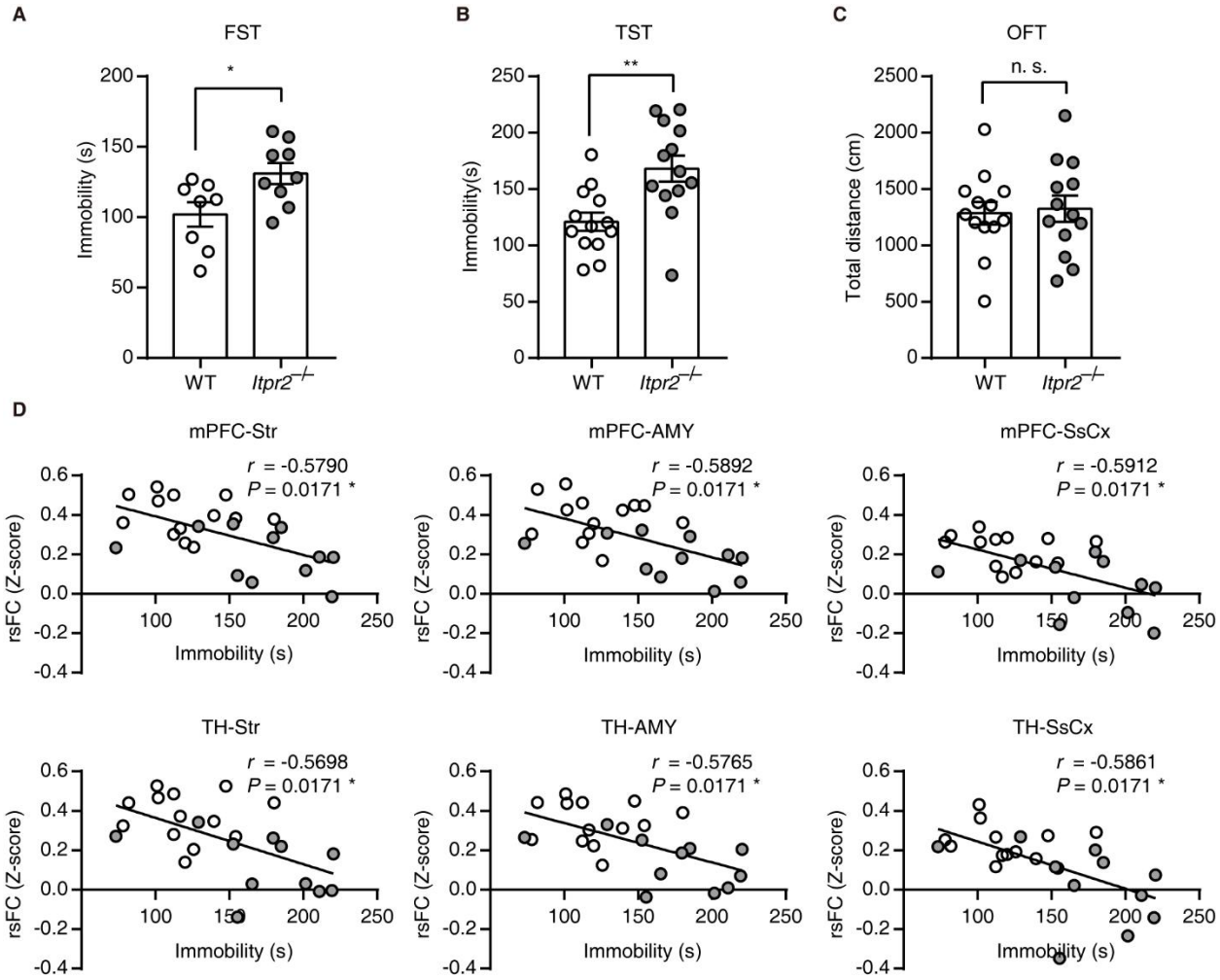

Fig. S1.

Correlation analysis between rsFC and immobility time. (**A-C**) Behavioral performances of WT and *Itpr2*$^{-/-}$ mice in forced swimming test (FST) (A, n = 8 and 9 for WT and *Itpr2*$^{-/-}$ mice, respectively), tail-suspension test (TST) (B, n = 13 mice in each group) and open field test (OFT) (C, n = 13 mice in each group). Data are expressed as mean ± s.e.m., *$P < 0.05$, **$P < 0.01$, n.s., no significance. Independent sample t test. (**D**) Significant correlations (Pearson's r) between the rsFC in the mPFC-Str, mPFC-AMY, mPFC-SsCx, TH-Str, TH-AMY and TH-SsCx pathways and the immobility time in TST. P-values were corrected with FDR. The white dots represent the data of WT mice (n = 13). The gray dots represent the data of *Itpr2*$^{-/-}$ mice (n =11). The reduced number of animals was due to the failure of fMRI acquisition.

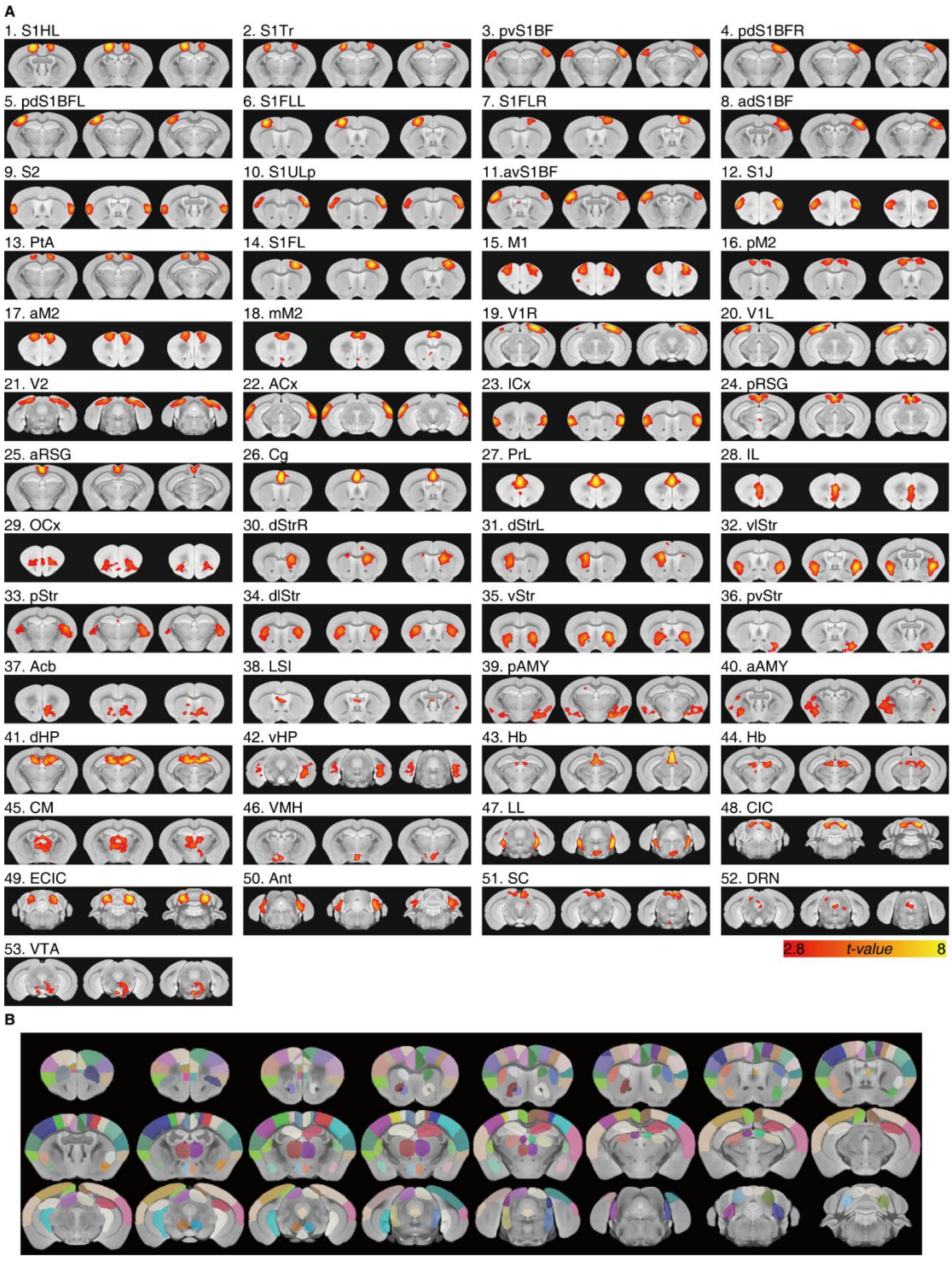

Fig. S2.

Data-driven spatial independent component analysis (ICA). (**A**) The 53 functional components. (**B**) Manually drawn ROI atlas encompassing 94 left-right symmetrical brain units (i.e. 47 brain regions), based on the 53 functional components and guided by the Paxinos and Watson Mouse Brain Atlas. For the abbreviation details, see table S1.

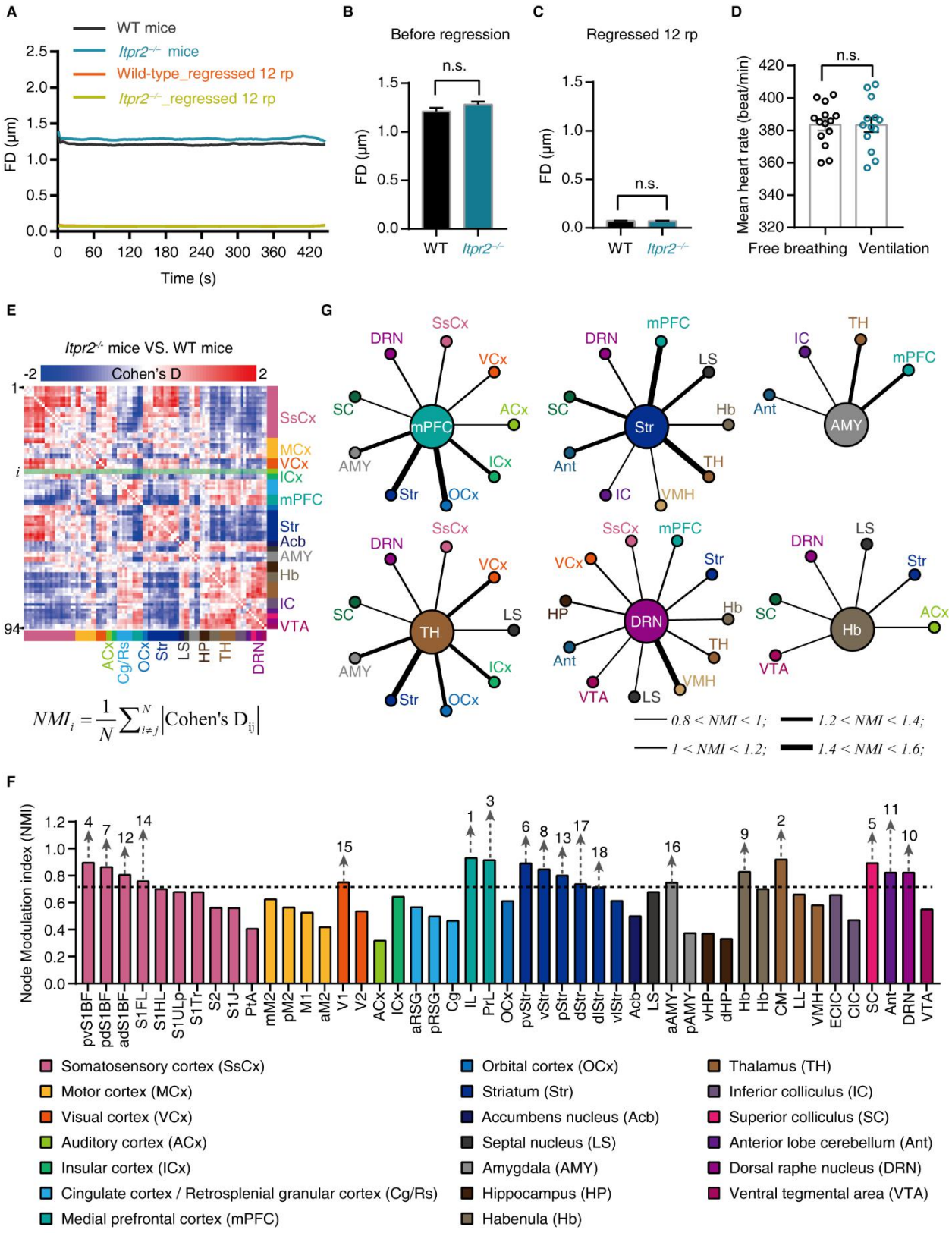
A
WT mice
Itpr2-/- mice
Wild-type_regressed 12 rp
Itpr2-/-_regressed 12 rp
FD (μm)
Time (s)
B
Before regression
n.s.
FD (μm)
WT
Itpr2-/-
C
Regressed 12 rp
n.s.
FD (μm)
WT
Itpr2-/-
D
n.s.
Mean heart rate (beat/min)
Free breathing
Ventilation
E
Itpr2-/- mice VS. WT mice
Cohen's D
SsCx
MCx
VCx
ICx
mPFC
Str
Acb
AMY
Hb
IC
VTA
ACx
Cg/Rs
OCx
Str
LS
HP
TH
DRN
NMI_i = 1/N Σ_{i≠j} |Cohen's D_ij|
G
0.8 < NMI < 1;
1 < NMI < 1.2;
1.2 < NMI < 1.4;
1.4 < NMI < 1.6;
F
Node Modulation index (NMI)
pvS1BF
pdS1BF
adS1BF
S1FL
S1HL
S1ULp
S1Tr
S2
S1J
PtA
mM2
pM2
M1
aM2
V1
V2
ACx
ICx
aRSG
pRSG
Cg
IL
PrL
OCx
pvStr
vStr
pStr
dStr
dlStr
vlStr
Acb
LS
aAMY
pAMY
vHP
dHP
Hb
Hb
CM
LL
VMH
ECIC
CIC
SC
Ant
DRN
VTA
Somatosensory cortex (SsCx)
Motor cortex (MCx)
Visual cortex (VCx)
Auditory cortex (ACx)
Insular cortex (ICx)
Cingulate cortex / Retrosplenial granular cortex (Cg/Rs)
Medial prefrontal cortex (mPFC)
Orbital cortex (OCx)
Striatum (Str)
Accumbens nucleus (Acb)
Septal nucleus (LS)
Amygdala (AMY)
Hippocampus (HP)
Habenula (Hb)
Thalamus (TH)
Inferior colliculus (IC)
Superior colliculus (SC)
Anterior lobe cerebellum (Ant)
Dorsal raphe nucleus (DRN)
Ventral tegmental area (VTA)

Fig. S3.

Whole-brain functional map showing the changed rsFC of *Itpr2*$^{-/-}$ mice. (**A**) The mean frame-wise displacements (FD) before and after regressing 12 head motion parameters (roll, pitch, yaw, translation in three dimensions, and the first derivative of each of those six parameters). (**B-C**) Quantitative analysis of the mean FD before and after regression. (**D**) Quantitative analysis of mean heart rate in free-breathing and mechanically ventilated mice (free-breathing: $n = 14$; ventilated: $n = 13$) in a 1-hour period after fixing the mice on the MRI-compatible cradle for 30 minutes. (**E**) Node modulation index (*NMI*), the mean effect size, was calculated as the average effect size in each brain region. (**F**) Brain regions were ranked in the order of their *NMI*. The rank number shown with the arrow above the bar graph indicates strong effect of altered rsFC in that brain region (*NMI* > 0.7, percentile standing > 75%). (**G**) Schematic diagram showing the changed rsFC with larger effect size (> 0.8) of 6 key brain regions associated with depression. For the abbreviation details, see table S1. Independent sample *t* test. Data are expressed as means ± s.e.m., n.s., no significance.

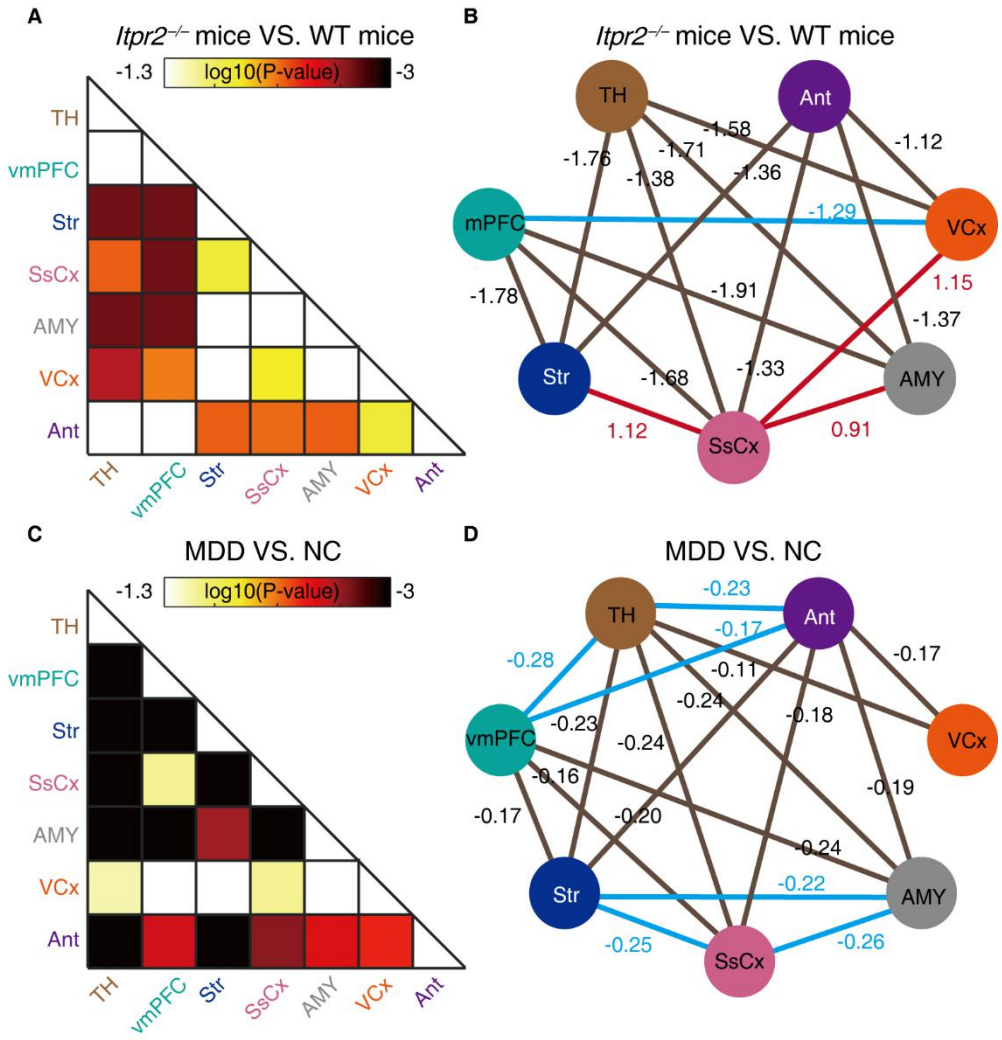

Fig. S4.

Comparison of altered rsFC within depression-related networks in *Itpr2*$^{-/-}$ mice and MDD patients. (**A, C**) Heat maps showing inter-group statistical comparisons of rsFC between *Itpr2*$^{-/-}$ and WT mice (Independent sample *t* test), and between MDD and NC subjects (Linear mixed models). Color-coded values represent the log *P*-values for group comparisons, $P < 0.05$, corrected with FDR. (**B, D**) Network graphs showing altered rsFC in *Itpr2*$^{-/-}$ mice and MDD patients. The value of each pathway represents the effect size (Cohen's D). Altered rsFC in both *Itpr2*$^{-/-}$ mice and MDD patients is shown in gray lines. Decreased rsFC specific to *Itpr2*$^{-/-}$ mice or MDD patients is shown in blue lines, while increased rsFC specific to *Itpr2*$^{-/-}$ mice or MDD patients is shown in red lines.

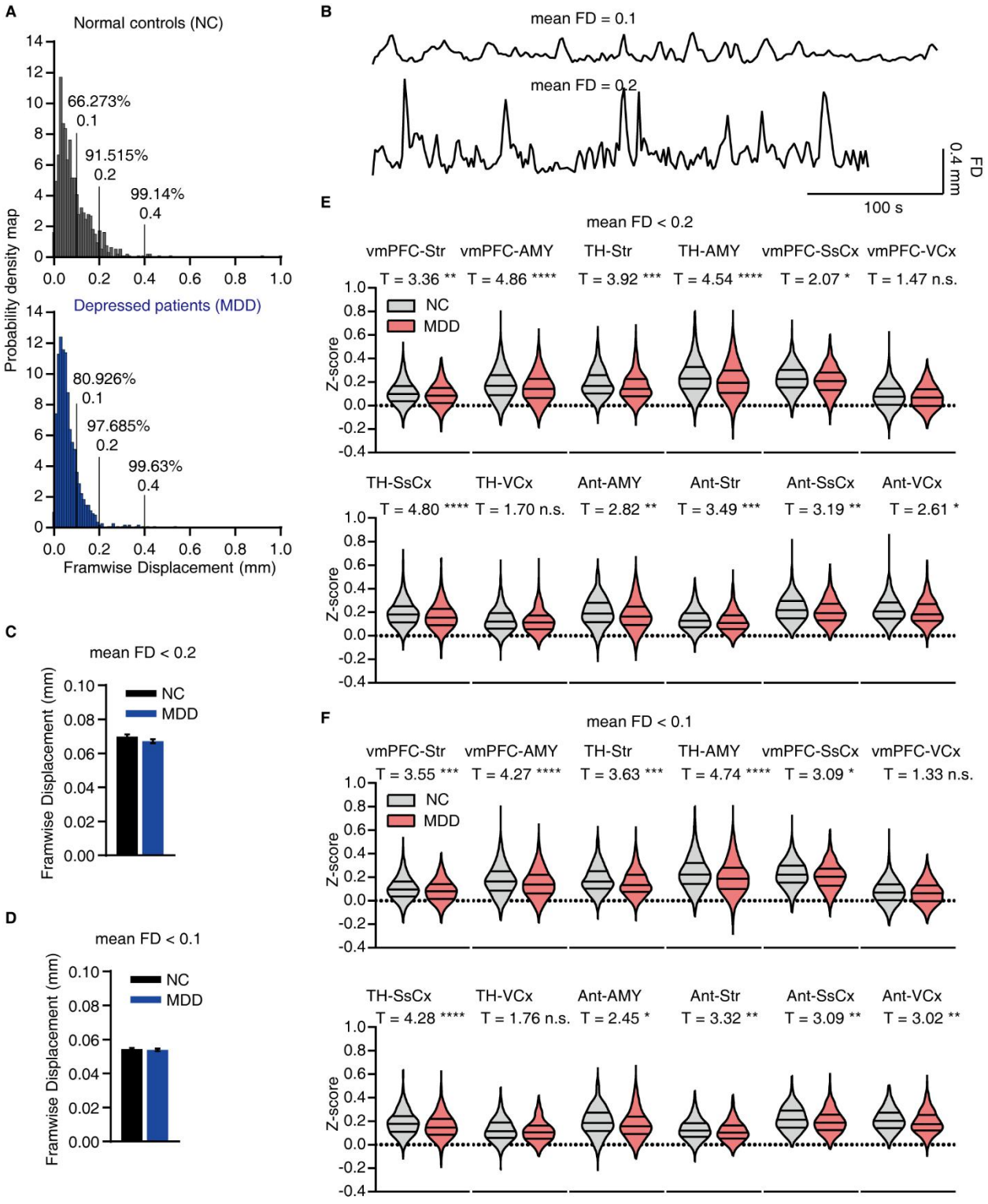

Fig. S5.

The altered rsFC in MDD patients stays constant under aggressive head motion control. (**A**) The probability density map of mean FD for 931 normal controls (upper panel) and 1080 depressed patients (low panel). In the two groups, the mean FD is less than 0.4 mm for the vast

majority (> 99%) of subjects. (**B**) Representative FD traces for low-motion (upper panel, mean FD = 0.1) and high-motion (low panel, mean FD = 0.2) subjects, respectively. (**C**) Comparison of mean FD between 1059 patients and 917 controls after excluding subjects with mean FD > 0.2 mm (Mann-Whitney U Test, $P = 0.156$). (**D**) Comparison of mean FD between 879 patients and 733 controls after excluding subjects with mean FD > 0.1 mm (Mann-Whitney U Test, $P = 0.764$). (**E-F**) Violin figures showing the distribution of rsFC for MDD patients and normal controls after excluding subjects with large head motion. Linear mixed models. *P*-values were corrected with FDR, $*P < 0.05$, $**P < 0.01$, $***P < 0.001$, $****P < 0.0001$, n.s., no significance.

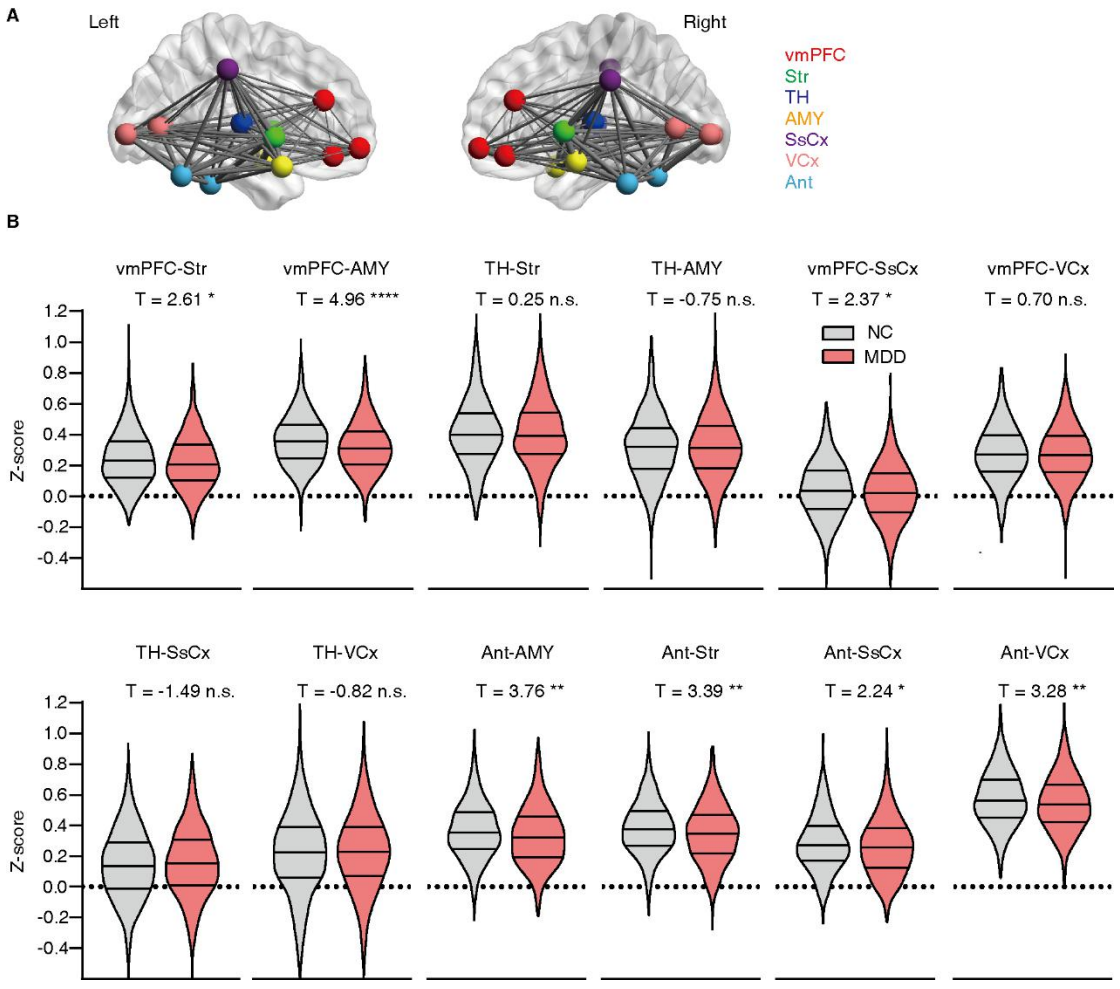

Fig. S6.

The validation analysis of MDD rsfMRI data using Craddock's functional clustering atlas. (**A**) Locations of ROIs generated from the Craddock's functional clustering atlas. (**B**) Violin figures showing the distribution of the rsFC for MDD and NC subjects. Linear mixed models. Multiple comparison was corrected with FDR, *$P < 0.05$, **$P < 0.01$, ***$P < 0.001$, ****$P <$ 0.0001, n.s., no significance. See table S4 for MNI coordinates for ROIs in (A).

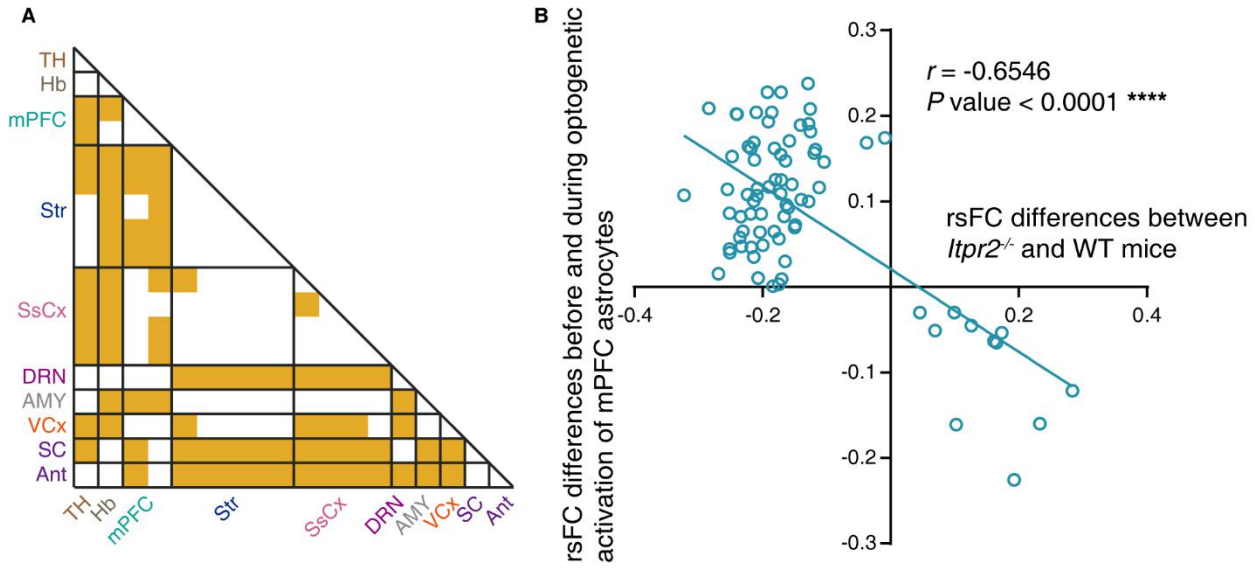

Fig. S7.

Correlation analysis between *Itpr2* knockout effect and the effect of optogenetic activation of mPFC astrocytes. (**A**) Heat map showing pathways with rsFC changes in opposite directions (51%, 78 out of 153 pathways) due to *Itpr2* knockout and optogenetic activation of mPFC astrocytes. (**B**) Correlation analysis between the rsFC differences of *Itpr2*$^{-/-}$ and WT mice, and the rsFC differences of *Itpr2*$^{-/-}$ mice before and during optogenetic activation of mPFC astrocytes (78 pathways). Among them, 67 out of 78 pathways showed rsFC decreases with *Itpr2* knockout but increases with astrocyte activation (the second quadrant), whereas the remaining pathways showed rsFC increases with *Itpr2* knockout but decreases with astrocyte activation (the fourth quadrant).

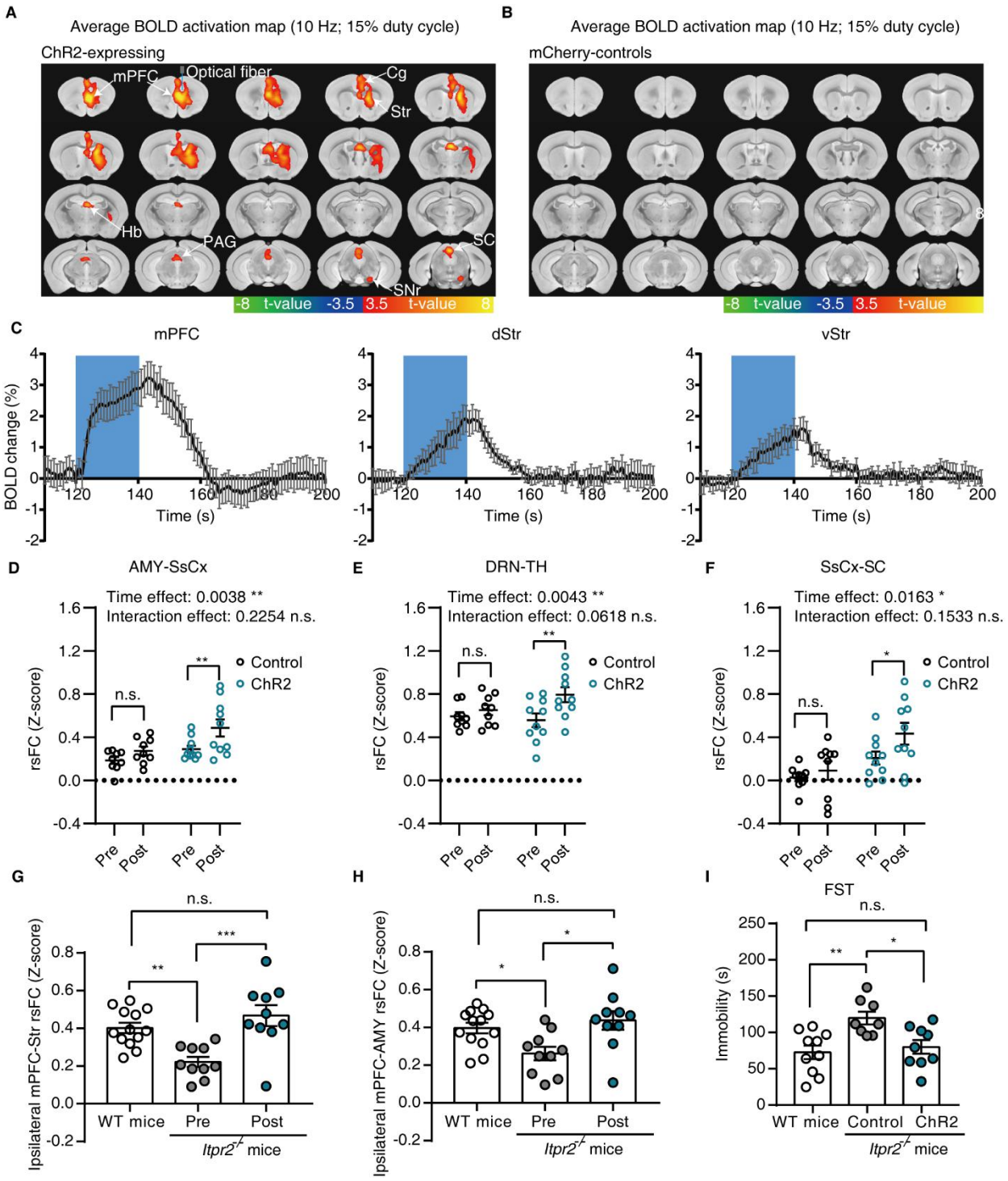

Fig. S8.

Optogenetic activation of mPFC neurons drives local and downstream positive BOLD. (**A-B**) BOLD activations were observed in ChR2-expressing mice, but not in mCherry controls (n = 10 and 9 for ChR2 and control mice, respectively). (**C**) Average BOLD signal profiles extracted from the mPFC, dStr and vStr of ChR2-expressing mice. (**D-F**) Quantitative analyses of the rsFC in ipsilateral AMY-SsCx, DRN-TH and SsCx-SC pathways before and after optogenetic

stimulation. Two-way ANOVA with Sidak's multiple comparison test. (**G-H**) Quantification of ipsilateral mPFC-Str and mPFC-AMY rsFC in WT (without optogenetic stimulation, $n = 13$) and *Itpr2*$^{-/-}$ mice (before and after optogenetic activation of mPFC neurons, $n = 10$). The rsFC was calculated using the ICA-detected ROIs within depression-related networks in ipsilateral hemisphere of the brain. (**I**) Behavioral performances of WT and *Itpr2*$^{-/-}$ mice in FST ($n = 10$, 8 and 9 for WT, *Itpr2*$^{-/-}$ Pre and *Itpr2*$^{-/-}$ post mice, respectively). One-way ANOVA followed by Sidak's multiple comparison test for (G-I). All data are expressed as means ± s.e.m., $*P < 0.05$, $**P < 0.01$, $***P < 0.001$, n.s., no significance.

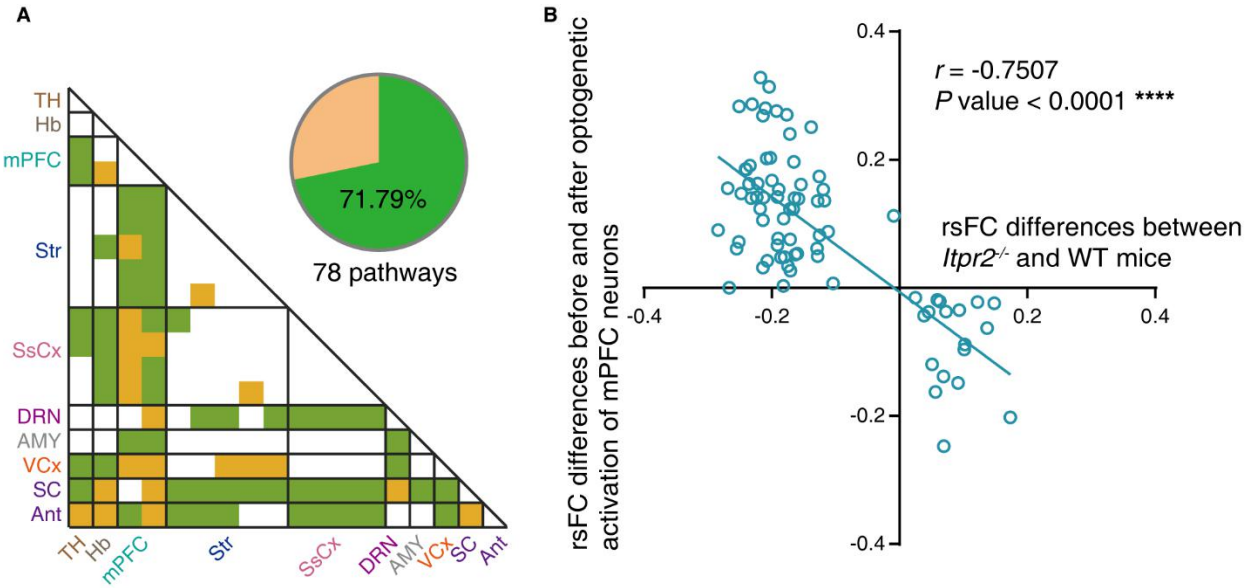

Fig. S9.

Correlation analysis between *Itpr2* knockout effect and the effect of optogenetic activation of mPFC neurons. (**A**) Heat map (yellow and green) showing pathways with rsFC changes in opposite directions (51%, 78 out of 153 pathways) due to *Itpr2* knockout and optogenetic activation of mPFC neurons. In these 78 pathways, optogenetic activation of mPFC neurons caused the same direction of rsFC changes as optogenetic activation of mPFC astrocytes in 71.79% (56 out of 78) pathways, shown in green. (**B**) Correlation analysis between the rsFC differences of *Itpr2*$^{-/-}$ and WT mice, and the rsFC differences of *Itpr2*$^{-/-}$ mice before and after optogenetic activation of mPFC neurons (78 pathways). Among them, 60 out of 78 pathways showed rsFC decreases with *Itpr2* knockout but increases with mPFC neurons activation (the second quadrant), whereas the remaining pathways showed rsFC increases with *Itpr2* knockout but decreases with mPFC neurons activation (the fourth quadrant).

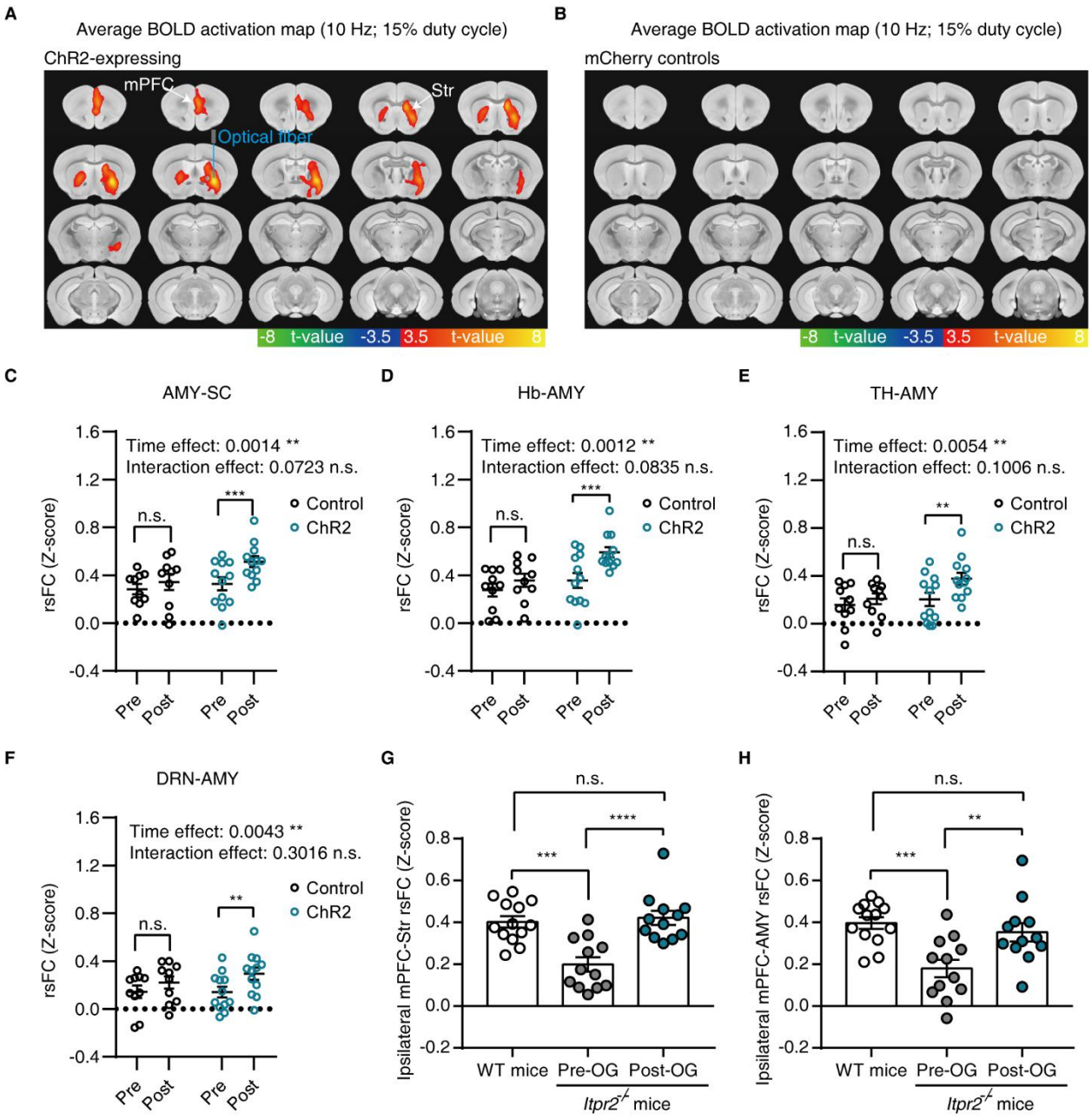

Fig. S10.

Optogenetic activation of mPFC-to-striatum projection rescues mPFC-Str and mPFC-AMY rsFC of *Itpr2*$^{-/-}$ mice. (**A-B**) Blue light evoked BOLD activation in the mPFC-Str pathway in ChR2-expressing mice, but not in mCherry controls (n = 12 and 10 for ChR2 and control mice, respectively). (**C-F**) Quantitative analyses of the rsFC in ipsilateral AMY-SC, Hb-AMY, TH-AMY and DRN-AMY pathways before and after optogenetic stimulation. Two-way ANOVA with Sidak's multiple comparison. (**G-H**) Quantification of ipsilateral mPFC-Str and mPFC-AMY rsFC in WT (without optogenetic stimulation, n = 13) and *Itpr2*$^{-/-}$ mice (before and after optogenetic activation of mPFC neurons, n = 12). The rsFC was calculated using the ICA-detected ROIs within depression-related networks in ipsilateral hemisphere of the brain. One-

way ANOVA followed by Sidak's multiple comparison test. All data are expressed as means ± s.e.m., *$P < 0.05$, **$P < 0.01$, ***$P < 0.001$, ****$P < 0.0001$, n.s., no significance.

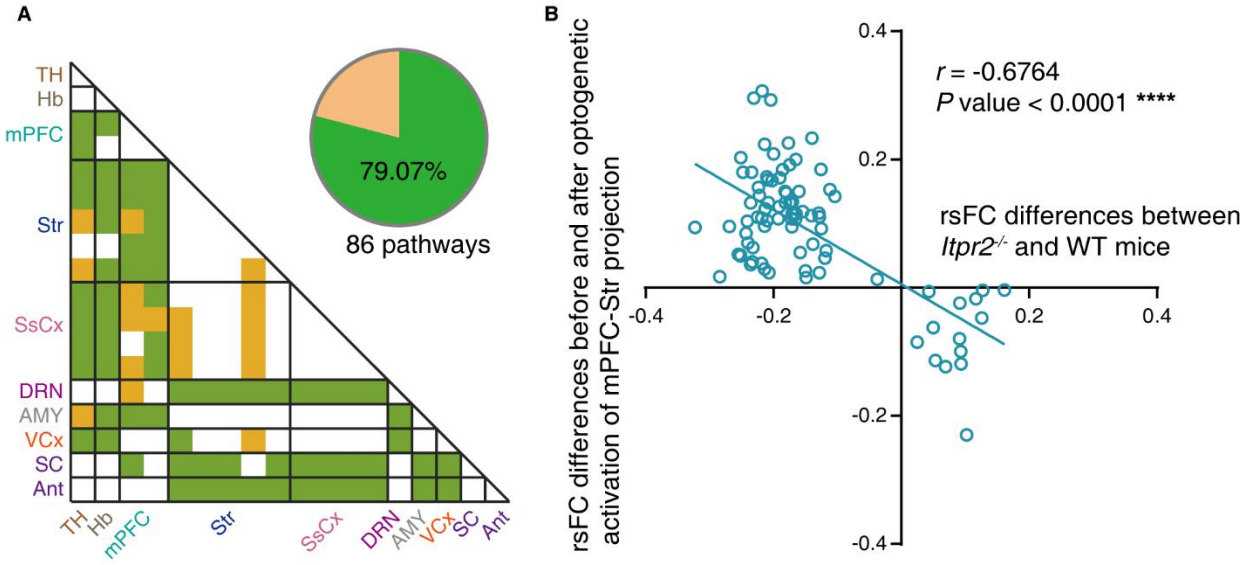

Fig. S11.

Correlation analysis between *Itpr2* knockout effect and the effect of optogenetic activation of mPFC-Str projection. (**A**) Heat map (yellow and green) showing pathways where rsFC changes in opposite directions (56%, 86 out of 153 pathways) due to *Itpr2* knockout and optogenetic activation of mPFC-Str projection. In these 86 pathways, optogenetic activation of mPFC-Str projection led to the same direction of rsFC changes as optogenetic activation of mPFC astrocytes in 79.09% (68 out of 86) pathways, shown in green. (**B**) Correlation analysis between the rsFC differences of *Itpr2*$^{-/-}$ and WT mice, and the rsFC differences of *Itpr2*$^{-/-}$ mice before and after optogenetic activation of mPFC-Str projection (86 pathways). Among them, 72 out of 86 pathways showed rsFC decreases with *Itpr2* knockout but increases with activation of the mPFC-Str projection (the second quadrant), whereas the remaining pathways showed rsFC increases with *Itpr2* knockout but decreases with activation of the mPFC-Str projection (the fourth quadrant).

Table S1. Brain components from spatial ICA.

See attached supplementary tables.

Table S2. Human samples of study sites in the present study, modified from Supplementary Table S3 of Yan et al (*32*).

See attached supplementary tables.

Table S3.

MNI coordinates for the human atlas-defined ROIs from the Dosenbach functional atlas and Automated Anatomical Labeling atlas. Note that our ROIs in depression-related networks correspond to multiple human atlas-defined ROIs.

ROI		MNI coordinates		
Our ROIs	**Corresponding human atlas-defined ROIs**	**x**	**y**	**z**
vmPFC	Ventromedial prefrontal cortex1	6	64	3
	Ventromedial prefrontal cortex2	9	51	16
	Ventromedial prefrontal cortex3	-6	50	-1
	Ventromedial prefrontal cortex4	-11	45	17
	Ventromedial prefrontal cortex5	8	42	-5
Str	Striatum1	-6	17	34
	Striatum2	-20	6	7
	Striatum3	14	6	7
	Striatum4	11	-24	2
TH	Thalamus1	-12	-3	13
	Thalamus2	-12	-12	6
	Thalamus3	11	-12	6
AMY	Amygdala1	-23.27	-0.67	-17.14
	Amygdala2	27.32	0.64	-17.5
SsCx	Somatosensory cortex1	-55	-22	38
	Somatosensory cortex2	-41	-31	48
VCx	Primary Visual cortex1	9	-76	14
	Primary Visual cortex2	15	-77	32
	Primary Visual cortex3	13	-91	2
Ant	Anterior lobe cerebellum1	-24	-54	-21
	Anterior lobe cerebellum2	-34	-57	-24
	Anterior lobe cerebellum3	-16	-64	-21
	Anterior lobe cerebellum4	21	-64	-22

Table S4.

MNI coordinates for the human atlas-defined ROIs from the Craddock's functional clustering atlas. Note that our ROIs in depression-related networks correspond to multiple human atlas-defined ROIs.

ROI		MNI coordinates		
Our ROIs	**Corresponding human atlas-defined ROIs**	**x**	**y**	**z**
vmPFC	Ventromedial prefrontal cortex	1	35	23
	Ventromedial prefrontal cortex	-1	41	-13
	Ventromedial prefrontal cortex	1	58	-8
Str	Striatum	26	3	-1
	Striatum	-29	3	3
TH	Thalamus	11	-18	8
	Thalamus	-9	-16	9
Amy	Amygdala	-20	-5	-17
	Amygdala	30	8	-20
SsCx	Somatosensory cortex	-57	-27	36
	Somatosensory cortex	55	-27	43
VCx	Primary Visual cortex	13	-93	1
	Primary Visual cortex	-12	-69	5
	Primary Visual cortex	7	-72	5
	Primary Visual cortex	-7	-91	1
Ant	Anterior lobe cerebellum	-29	-38	-31
	Anterior lobe cerebellum	20	-57	-26